Int. J. Nanosci. Nanotechnol., Vol. 19, No. 4, Dec. 2023, pp. 249-262
DOI: 10.22034/ijnn.2023.2000747.2365

Exploring the Nonlinear Optical Behaviour of InGaAs/GaAs Triple Quantum Wells via Structural Modulations and External Electric Fields

Muhammed Sayrac[1,*], Hassen Dakhlaoui[2,3], Miguel Eduardo Mora-Ramos[4] and Fatih Ungan[5]

[1]Department of Nanotechnology Engineering, Sivas Cumhuriyet University, P. O. Box 58140 Sivas, Turkey
[2]Nanomaterials Technology unit, Basic and Applied Scientific Research Center (BASRC), College of Science of Dammam, Imam Abdulrahman Bin Faisal University, P. O. Box 1982, 31441 Dammam, Saudi Arabia
[3]Department of Physics, College of Sciences for Girls, Imam Abdulrahman Bin Faisal University, Saudi Arabia
[4]Centro de Investigación en Ciencias-IICBA, Universidad Autonoma del Estado de Morelos, Ave. Universidad P. O. Box 51001, CP 62209, Cuernavaca, Morelos, Mexico
[5]Department of Physics, Sivas Cumhuriyet University, P. O. Box 58140 Sivas, Turkey

(*) Corresponding author: muhammedsayrac@cumhuriyet.edu.tr
(Received: 24 April 2023 and Accepted: 10 October 2023)

Abstract

The nonlinear optical properties of the InxGa1-xAs/GaAs triple quantum well structure are studied for different structure parameters and applied external electric field. Within the framework of the effective mass and envelope function approximations, the one-dimensional time-independent Schrödinger wave equation is solved using the diagonalization method to obtain the energy eigenvalues and eigenfunctions of the structure. The coefficients of nonlinear optical properties such as nonlinear optical rectification (NOR), second harmonic generation (SHG), and third harmonic generation (THG) of the structure are numerically evaluated from the corresponding expressions derived within the compact density matrix approximation. The influence of adjustable structure parameters and the applied external electric field affects the separation of subband energy levels and the magnitudes of dipole moment matrix elements. These changes in the electronic properties of the structure cause the NOR, SHG, and THG peak positions to shift towards lower or higher energy regions. It is expected that these results will enable the appropriate design of new optoelectronic devices.

Keywords: *InGaAs, Confinement potential, NOR, SHG, THG, Low dimensional system.*

1. INTRODUCTION

Investigation of low-dimensional carrier systems in quantum nanostructures has been performed for the last few decades due to their potential application in laser and optoelectronic technology [1-6]. Electron confinement in these structures results in the formation of a discrete energy spectrum [7-9]. The separation of energy levels is controlled by modifying the geometry of the structure in terms of potential barrier height, barrier thickness, and well depth, as well as by changing the quantum well (QW) shape through the application of external fields [10]. Variation of linear and nonlinear optical properties is observed as a result of the modification of the confining potential profile [10, 11]. Concerning second and third-order nonlinear responses, NOR, SHG, and THG coefficients have attracted attention due to their potential applications from infrared laser amplifiers to

photodetectors and from optical switchers to high-speed optical modulators [12].

In many cases, the manifestation of nonlinear optical properties in low-dimensional quantum structures is directly related to the asymmetry of the confinement potential shape [13-18]. The asymmetry of the quantum well potential allows the observation of high-order susceptibilities such as second-order [19] and third-order nonlinear ones [7, 20-22]. In accordance, Pöschl-Teller potential has been studied by several researchers [23-25]. Radovanovic et al. explored intersubband optical absorption [26]. In addition, Yuh et al. considered the case of a narrow QW inserted in a large one [27]. Besides, Feng et al. investigated the absorption of a five-step QW under applied external probes [28]. The mentioned QW potentials are tunable and solutions for allowed electron states are obtained by solving the corresponding Schrödinger equation [29]. These studies have explored the nonlinear optical properties of the low-dimensional structure.

Application of external fields (electric, magnetic, and intense laser field), as well as the suitable modification of structure parameters (well width, barrier thickness, and well depth) to achieve specific potential energy function configuration, significantly alter the linear and nonlinear optical properties in low-dimensional QW systems [30-36]. Theoretical and experimental investigations have demonstrated that the nonlinear optical properties strongly depend on the asymmetricity of the confinement potential shape [37-43]. For instance, the aimed potential structure could be fabricated by controlling the width/depths of the QW and by the applied external electric field. These parameters tilt the band profile of the structure [4, 44, 45].

The paper aims to examine the NOR, SHG, and THG coefficients in a triple InGaAs/GaAs QW structure. The effects of the change of structure parameters and applied external electric fields are focused on in this work. The triple InGaAs/GaAs QW is an important semiconductor device that has many potential applications in optoelectronics and quantum computing. For example, high-efficiency light-emitting diodes (LEDs) in the infrared range, high-speed photodetectors, quantum computing due to its ability to confine electrons in a small space, and nanophotonics. Overall, the triple InGaAs/GaAs quantum well structure is an important semiconductor device that has many potential applications in optoelectronics, quantum computing, and nanophotonics. Its unique properties make it an important area of research and development in the semiconductor industry. However, understanding the carrier dynamics in these structures can be complex and challenging. Simulation techniques such as computational modeling and numerical simulations can be used to study the behavior of carriers in triple quantum well structures. These simulations can provide detailed information about the energy levels, carrier lifetimes, and other properties of the structure, which can help in the design and optimization of optoelectronic devices based on these structures.

For the above-mentioned features of the QW structure, the investigation of the nonlinear optical properties of the InGaAs/GaAs QW structure is studied in detail. To achieve this, a numerical simulation is performed to obtain NOR, SHG, and THG coefficients at different structure parameters and external electric fields. For this, firstly, the energy eigenvalues and eigenfunctions of an electron surrounded in the conduction band of the structure are obtained within the framework of the effective mass and envelope function approach for different structural parameters and applied external electric field. Then, by using these energy eigenvalues and eigenfunctions, the NOR, SHG, and THG coefficients of the structure were obtained numerically using the compact density matrix approach. The organization of the paper is as follows: Section 3 draws a theoretical framework.

Section 3 discusses the numerical results. Section 4 presents the conclusion of the paper.

2. THEORY

The $In_xGa_{1-x}As/GaAs$ QW structure is schematically depicted in Fig. 1. The configuration of the structure stetting: z_1=5nm, z_2-z_1 = Lw_L, z_3-z_2 = Lb_L, z_4-z_3 = Lw_c, z_5-z_4 = Lb_R, z_6-z_5 = Lw_R, z_7-z_6= 5nm. V_0= 188meV (well depth for x=0.2), V_1= 234meV (well depth for x=0.25). Lw_L, Lw_c, and Lw_R are left, center, and right well width, and Lb_L, and Lb_R are left and right barrier thickness. By controlling the z values, the structure profile (well width and barrier thickness) is changed. In addition, the applied external electric field also changes the confinement potential profile of the structure. These modifications in the shape of the confinement potential cause variations between electron energy levels. The Hamiltonian of an electron confined in the proposed structure in the presence of the z-oriented electric field within the framework of effective mass and parabolic band approximations are given by [46-48].

$$H = \frac{\vec{p}_e^{\,2}}{2m^*} + V(z) - e\vec{Fz} \tag{1}$$

where m^* and P_e are the electron effective mass and the electron momentum. F corresponds to the external electric field. With all this, the expression for $V(z)$, the confinement potential for the electron in the z-direction is:

$$V(z) = \begin{cases} V_0 & 0 < z < z_1 \\ (V_1 - V_0) & z_1 < z < z_2 \\ V_0 & z_2 < z < z_3 \\ 0 & z_3 < z < z_4 \\ V_0 & z_4 < z < z_5 \\ (V_1 - V_0) & z_5 < z < z_6 \\ V_0 & z_6 < z < z_7 \end{cases} \tag{2}$$

In numerical calculation, the wave function and subband energy values of a single electron are obtained by using the diagonalization method [49]. In this method, the single-electron wave function $\psi(z)$ is obtained for infinite quantum well width (L_∞), which is large compared to the triple QW widths. The wave function under the influence of a zero electric field (F) describing the structure consists of the complete set is given

$$\psi(z) = (\sqrt{2\alpha})\sum_{n=1}^{\infty} C_n \sin(n\pi(z\alpha + \frac{1}{2})) \tag{3}$$

where C_n is coefficients and $\alpha = {}^{1}/_{L_\infty}$.

After the wavefunctions and the energies are determined, the nonlinear optical rectification (NOR), second-harmonic generation (SHG), and third-harmonic generation (THG) are analytically expressed under the density matrix approach and iterative method.

To derive the working expressions for NOR, SHG, and THG coefficients, it is assumed the incidence of a polarized electromagnetic field with frequency ω on the system:

$$E(t) = E_0 e^{i\omega t} + E_0 e^{-i\omega t} \tag{4}$$

The time evolution of one electron density operator ρ is given by [10, 50]:

$$\frac{\partial \rho}{\partial t} = \frac{1}{i\hbar}[H_0 - qxE(t), \rho] - \Gamma(\rho - \rho^{(0)}) \tag{5}$$

where H_0 is the Hamiltonian for the system without the electromagnetic field ($E(t)$). $\rho^{(0)}$ is the unperturbed density matrix operator and Γ is responsible for the electron-phonon interaction and collisions among electrons. Eq. (5) is solved by using the iterative approach [51]:

$$\rho(t) = \sum_n \rho^{(n)}(t),$$
$$\frac{\partial \rho_{ij}^{(n+1)}}{\partial t} = \frac{1}{i\hbar}[H_0, \rho^{(n+1)}] - \Gamma_{ij}\rho_{ij}^{(n+1)} - \frac{1}{i\hbar}[qx, \rho^{(n)}]_{ij}E(t) \tag{6}$$

The use of this density operator determines the macroscopic electronic polarization of the system ($P(t)$) and leads to [51]:

$$P(t) = \varepsilon_0\chi_\omega^{(1)}E_0 e^{i\omega t} + \varepsilon_0\chi_0^{(2)}E_0^2 + \varepsilon_0\chi_{2\omega}^{(2)}E_0^2 e^{2i\omega t} + \varepsilon_0\chi_{3\omega}^{(3)}E_0^3 e^{3i\omega t} + \ldots \tag{7}$$

here ε_0 is the permittivity of the free space. $\chi_{\omega}^{(1)}$, $\chi_{0}^{(2)}$, $\chi_{2\omega}^{(2)}$ and $\chi_{3\omega}^{(3)}$ are the linear, optical rectification, second harmonic generation, and third harmonic generation susceptibilities, respectively. Rightfully considering not very intense incident radiation, Eq. (7) represents a perturbation expansion. From this formalism, the analytical expression for the optical rectification, second and third harmonic generation coefficients are derived [19, 52, 53]:

$$\chi_0^{(2)} = \frac{4e^3\rho_v}{\varepsilon_0\hbar^2} M_{01}^2 \delta_{01} \frac{\omega_{10}^2(1+\Gamma_2/\Gamma_1)+(\omega^2+\Gamma_2^2)(\Gamma_2/\Gamma_1-1)}{[(\omega_{10}-\omega)^2+\Gamma_2^2][(\omega_{10}+\omega)^2+\Gamma_2^2]} \tag{8}$$

$$\chi_{2\omega}^{(2)} = \frac{e^3\rho_v}{\varepsilon_0\hbar^2} \frac{M_{01}M_{12}M_{20}}{(\omega-\omega_{10}-i\Gamma_3)(2\omega-\omega_{20}-i\Gamma_3)} \tag{9}$$

$$\chi_{3\omega}^{(3)} = \frac{e^3\rho_v}{\varepsilon_0\hbar^2} \frac{M_{01}M_{12}M_{23}M_{30}}{(\omega-\omega_{10}-i\Gamma_3)(2\omega-\omega_{20}-i\Gamma_3)(3\omega-\omega_{30}-i\Gamma_3)}. \tag{10}$$

where ρ_v is a three-dimensional concentration of electrons involved in the transition, and $M_{ij} = \langle \psi_i | z | \psi_j \rangle, (i,j = 0,1,2,3)$ is the off-diagonal matrix element. δ_{10} is $\delta_{10} = |M_{00} - M_{11}|$. $\omega_{ij} = (E_i - E_j)/\hbar$ is the transition frequency, and $\Gamma_k = 1/T_k, (k = 1,2,3)$ is the coefficient that is associated with the lifetime of the electron involved in transitions. For the equation (8-10), for SHG and THG, both the individual energy intervals and the overall change of energy levels (ΔE_{12}, ΔE_{20}, ΔE_{23}, ΔE_{30}) can collectively impact the shift direction. These processes involve multiple energy differences, so analyzing how each energy interval changes is important for predicting whether a blue or red shift will occur. However, for NOR, where a single energy interval (ΔE_{01}) is involved, the analysis of this energy difference is enough to comprehend the shift.

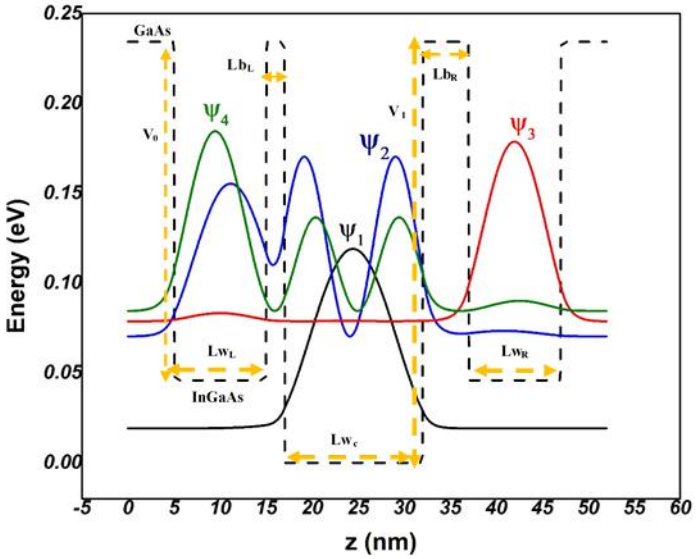

Figure 1. *Demonstration of confinement potential profile and allowed conduction band states presented through the corresponding probability densities.*

2. RESULT AND DISCUSSION

The input parameters for numerical calculation follow as [54, 55]: the effective mass of an electron is $m_e^* = 0.059m_0$ (m_0 is the free electron mass). The universal constants are $c = 3 \times 10^8 m/s$, $e =$

1.602×10^{-19} C, $\hbar = 1.056 \times 10^{-34}$Js $\rho_v = 3 \times 10^{22} m^{-3}$, $\mu = 4\pi \times 10^{7} Hm^{-1}$, $\varepsilon = 12.58$, $\varepsilon_0 = 8.854 \times 10^{-12}$, $\Gamma = 1{,}3{,}5$ THz and $n_r = 3.9$. The indium concentration (x) in the InGaAs alloy determines the discontinuity of the conduction band on the structure [56]

$$V_0^{InGaAs} = \%60(E_g^{GaAs} - E_g^{InGaAs}), \quad (11)$$

where $E_g^{InGaAs} = (E_g^{GaAs} - 1619x - 555x^2)$meV, $E_g^{GaAs} = 1424$meV. As previously stated, by considering Eq. (11), the potential depths for the center well (V_1) and side wells (V_0) are 234meV (x=0.25) and 189meV (x=0.20), respectively. With the use of small *In* contents and rather wide well regions, we are avoiding the influence of the lattice strain effect on the spectrum.

The effects of the structure parameters and the applied external electric field on the triple $In_xGa_{1-x}As/GaAs$ QW system are investigated. Fig. 1 contains the schematic plots of the lowest four electron states under zero applied field conditions. According to the chosen configuration, ground state wavefunction is completely confined within the central well. The first excited state is somewhat pushed toward the left well due to the orthogonality relation between the first excited state and the ground state. However, the second excited wave function is mainly localized in the central well and presents a penetration in the left one. Such a spatial separation observed in the profile of these wavefunctions is useful to control the dipole matrix elements. This leads to the best modulation of the NOR, SHG, and THG coefficients.

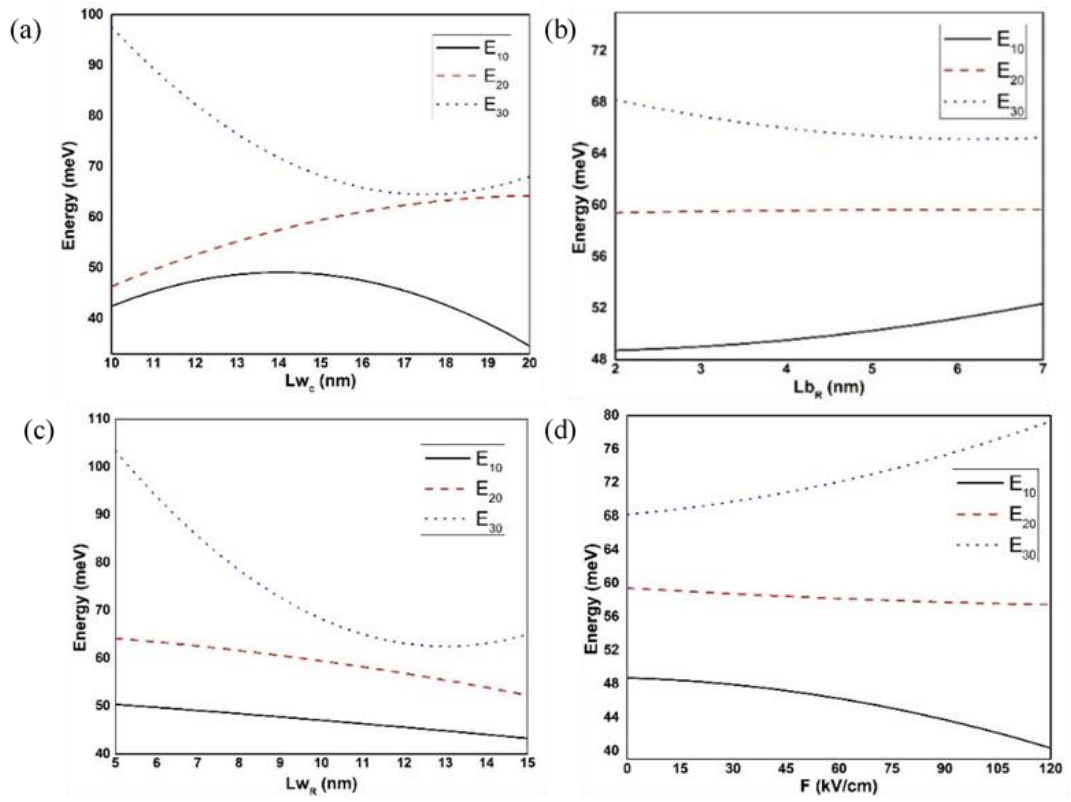

***Figure 2**. The first three eigenenergies of triple quantum well as a function of structural parameters of (a) central quantum well width (Lw_c), (b) right barrier thickness (Lb_R) (c) right quantum well width (LW_R), and (d) applied external electric field (F).*

Figure 2 shows the variation of the energy difference between the ground state and the first three excited states for different values of structure parameters (Lw_c, Lb_R, Lw_R) and applied external electric field (F).

In Fig (2a), we observe the variation of E_{10}, E_{20}, E_{30} as a function of the central well width. It appears that the E_{10} and E_{30} display an opposite variation. In fact, E_{10} increases slowly with Lw_c and then decreases, however E_{30} decreases from 100 meV (Lw_c = 10 nm) until it reaches a minimum of around 65 meV at (Lw_c = 18 nm) and then increases gradually. However, E_{20} rises slowly from 48meV to 60meV. All these variations are useful to discuss the red and blue shifts that may be observed in the NOR, SHG, and THG coefficients. In Fig (2b) we display the impact of the right barrier width (Lb_R) on E_{10}, E_{20}, E_{30} variations. It is shown that the augmentation of (Lb_R) does not affect significantly the energy separations. For instance, we remark that E_{20} is practically constant for all values of (Lb_R). So we can conclude that the energy variation is more sensitive to the width variation of the quantum well than that of the right barrier. In Fig (2c), the increase of right quantum well-width (Lw_R) reduces the energy separations E_{10}, E_{20}.However, E_{30} presents a strong reduction at first, and then it starts to increase with (Lw_R). The effect of the electric field on the energy separations is shown in Figure (2d). It is clear that E_{30} increases (blue shift) with all values of the electric field intensity contrarily to the previous cases when it shows two shifts (red and blue).

Table 1. *Dipole moment matrix elements for different confinement parameters (a)- (c) and (d) applied external electric field.*

(a)

Lw_c (nm)	M_{00} (nm)	M_{11} (nm)	M_{10} (nm)	M_{21} (nm)	M_{20} (nm)	M_{32} (nm)	M_{30} (nm)
10	22.0250	22.0126	2.3734	11.3716	0.0013	4.2658	2.009
15	24.5250	24.5233	3.3711	9.0355	6.30e-04	11.1464	1.3888
20	27.025	27.025	4.4428	4.4743	7.54e-05	15.4743	0.1004

(b)

Lb_R (nm)	M_{00} (nm)	M_{11} (nm)	M_{10} (nm)	M_{21} (nm)	M_{20} (nm)	M_{32} (nm)	M_{30} (nm)
2	24.5250	24.5233	3.3711	9.0355	0.006301	11.1464	1.3888
5	24.4072	19.2335	3.170	3.9247	0.0633	5.2643	1.5992
7	24.4037	18.8294	3.0593	1.5073	0.0278	2.0752	1.6123

(c)

Lw_R (nm)	M_{00} (nm)	M_{11} (nm)	M_{10} (nm)	M_{21} (nm)	M_{20} (nm)	M_{32} (nm)	M_{30} (nm)
5	24.5023	24.5060	3.3451	7.0488	1.3683	3.9598	0.1388
10	24.5023	24.5060	3.0711	9.0355	0.063	11.1464	1.3888
15	24.5023	24.5060	2.9375	7.5110	2.5865	8.2665	1.4383

(d)

F(kV/cm)	M00 (nm)	M11 (nm)	M10 (nm)	M21 (nm)	M20 (nm)	M32 (nm)	M30 (nm)
0	24.5250	24.5233	3.3711	9.0355	0.001	11.1464	1.3888
60	24.2095	22.4747	2.9419	7.9811	1.9763	7.2899	0.8900
120	23.8842	22.5546	2.4356	5.7171	2.7193	4.8256	0.4911

The dipole moment matrix elements values are responsible for the amplitude of the resonant peaks in each case, Table 1. Accordingly, Fig. 3 exhibits the NOR coefficient as a function of incident photon energy, with three different values of structure parameters. From Fig. 3(a) it is noticed that the variation of the center well width (Lw_c) initially produces a blue shift and then a red shift with the increment of Lw_c. This variation is seen from a black solid line in Figure 2 (a). The ground state and first excited state energy difference initially start increasing and then decreasing with the increment of center well width. The magnitude of the optical

rectification coefficient has been raised. The amplitude increment is attributed to the M_{10} dipole moment matrix element, which increases as Lw_c augments. From Fig. 3(b), nonlinear optical rectification shifts to higher energy levels with the increment of the barrier thickness (Lb_R). This blue shift is due to the increment of E_{10} with Lb_R which is shown by the black solid line in Fig. 2 (b). In this case, NOR response decreases in magnitude following the behavior of the dipole moment matrix element (M_{10}) with Lb_R. In addition, Fig. 3(c) shows the NOR coefficient red-shifted with the widening of the right well (Lw_R) since E_{10} decreases with an increment of Lw_R in Fig 2(c). Likewise, the dipole moment matrix element (M_{10}) diminishes with augmenting Lw_R, with the consequent effect on the amplitude of the optical rectification coefficients.

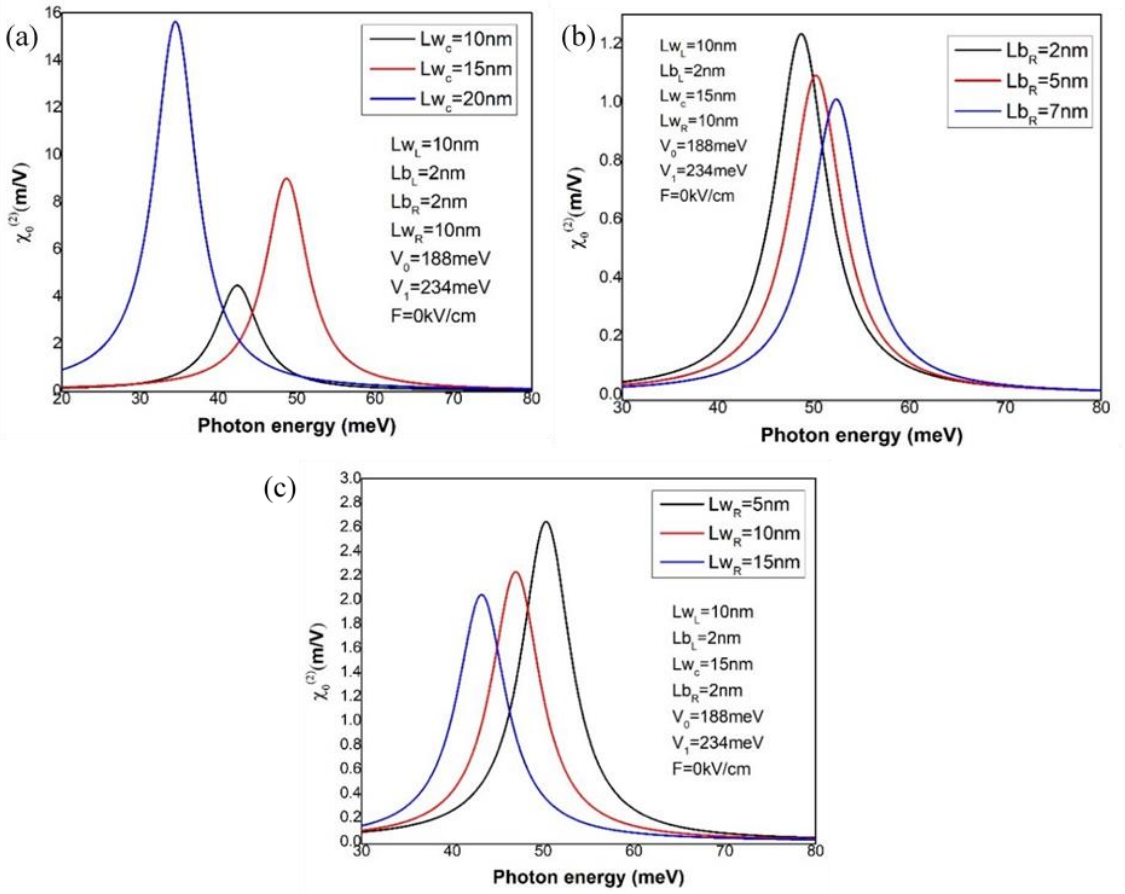

Figure 3. *Nonlinear optical rectification coefficient as a function of incident light energy for different sets of structural parameters (a) Lw_c (b) Lb_R (c) Lw_R.*

The influence of the applied static electric field on the NOR coefficient appears in Fig. 4 as a function of incident light energy, for three different values of field intensity. The increment of F causes the decrement of the energy difference between the ground state and the first excited state energy difference, as shown by the black solid line in Fig. 2(d). The applied electric field causes the redshift of the optical rectification coefficients. The amplitude of the NOR coefficient decreases since the dipole moment matrix element (M_{10}) also diminishes with the increment of the applied electric field. The decrease of (M_{10}) is attributed to the reduction in the overlap between the ground and first excited wavefunctions.

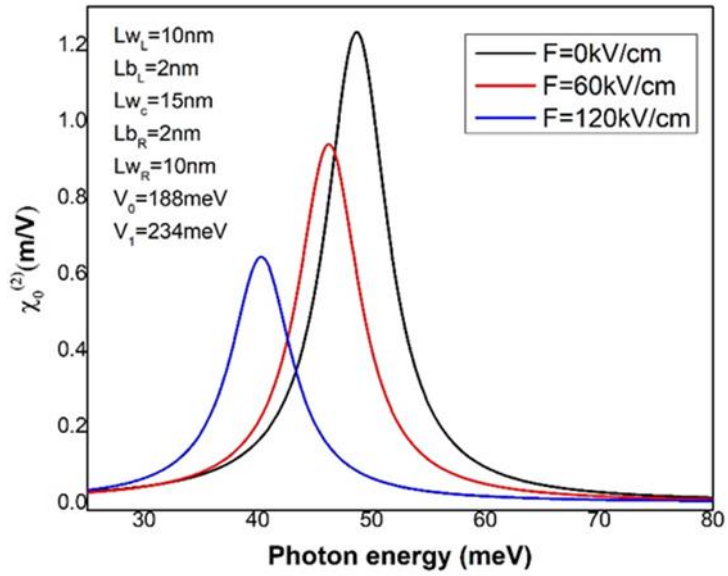

Figure 4*. Nonlinear optical rectification coefficient as a function of incident light energy, for three different external electric field values.*

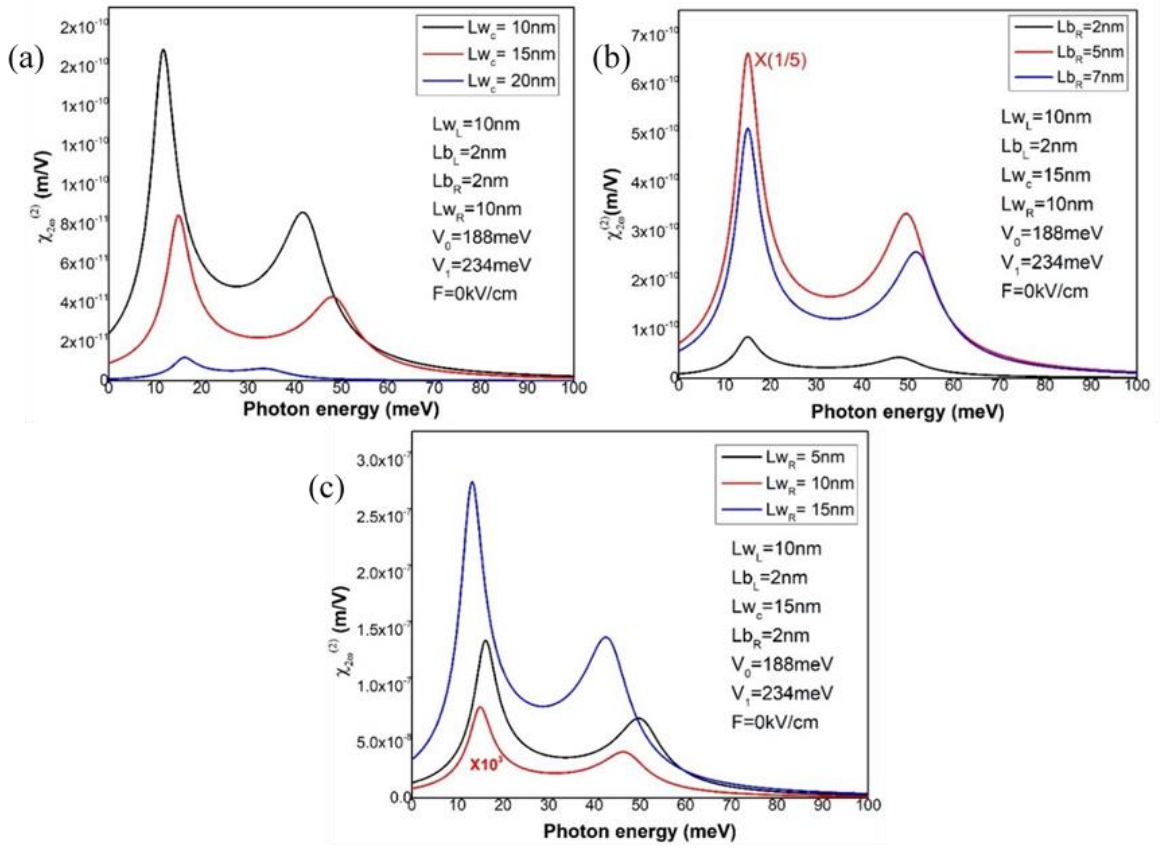

Figure 5. *Second harmonic generation coefficient as a function of incident light energy for different sets of structure parameters (a) Lw_c (b) Lb_R (c) Lw_R.*

The second harmonic coefficient has been presented as a function of incident photon energy for three different structure parameters, i.e. Lw_c, Lb_R, and Lw_R, respectively. The resonant peak of optical SH coefficients moves to the higher energy region by increasing the center well width (Lw_c), as shown in Fig. 5(a). The involved energy variation with the change of Lw_c is seen from the red dashed line in Figure

2(a). In addition, the magnitude (~$M_{01}M_{12}M_{20}$) of the SHG coefficients decreases with increasing Lw_c, since the product of dipole moment matrix elements reduces as well. Figure 5(b) presents the SHG coefficient for different right well barriers (Lb_R). The position of the main resonant SHG coefficient peak does not change much since the energy difference for different Lb_R values is stable, as noticed from the red dashed line in Fig. 2(b). On the other hand, the SHG peak amplitude drastically rises with the increment of Lb_R due to the increment of the product of the dipole moment matrix elements. Figure 5(c) demonstrates the SHG coefficient for different values of Lw_R. The energy difference between the ground state and second excited states decreases with the increment of Lw_R. This decrement results in the redshift of the resonant SHG coefficient peak for different Lw_R values, the red dashed line in Figure 2 (c). The amplitude of the SHG peak increases with the increment of Lw_R values since the product of the dipole moment matrix element also augments.

The applied external electric field (F) tilts the confinement potential profile, which directly affects the displacement of the electron inside the quantum well. The electron is placed for different energy states, and the difference between the energy states decreases or increases as a result of the applied electric field. In Fig. 6, the variation of the SHG coefficient is presented exposing the influence of this external probe. Due to the modification of confining potential, the energy difference between the ground state and the first two excited state (E_{10} and E_{20}) decrease. E_{20} slightly decreases, and the E_{10} decrement is noticeably seen in Fig. 2(d). All this reflects in almost no change of the main resonant peak position (very slightly towards red) and a noticeable shift to the red of the secondary peak. The amplitude of the SHG resonant peak augments with the increment of the F field because the dipole moment matrix elements increase with the increment of the F.

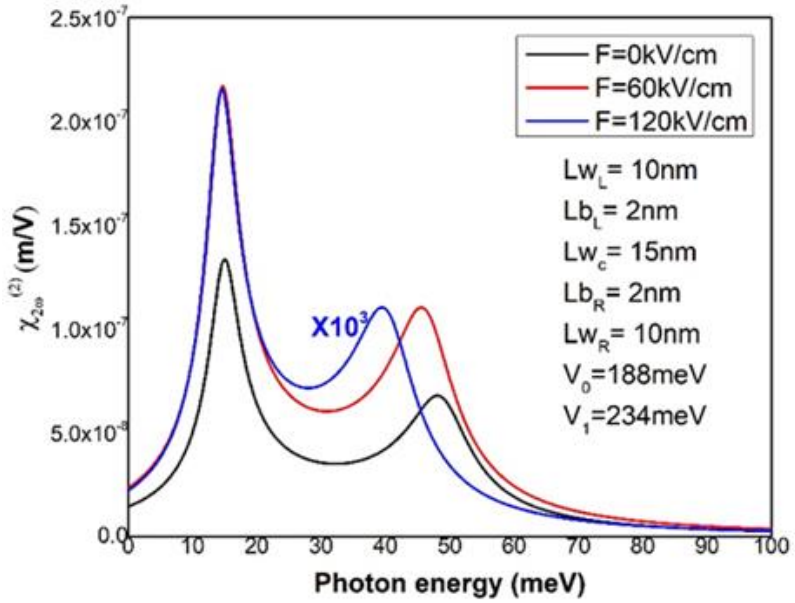

Figure 6. *Second harmonic generation coefficient as a function of incident light energy for different external electric field values.*

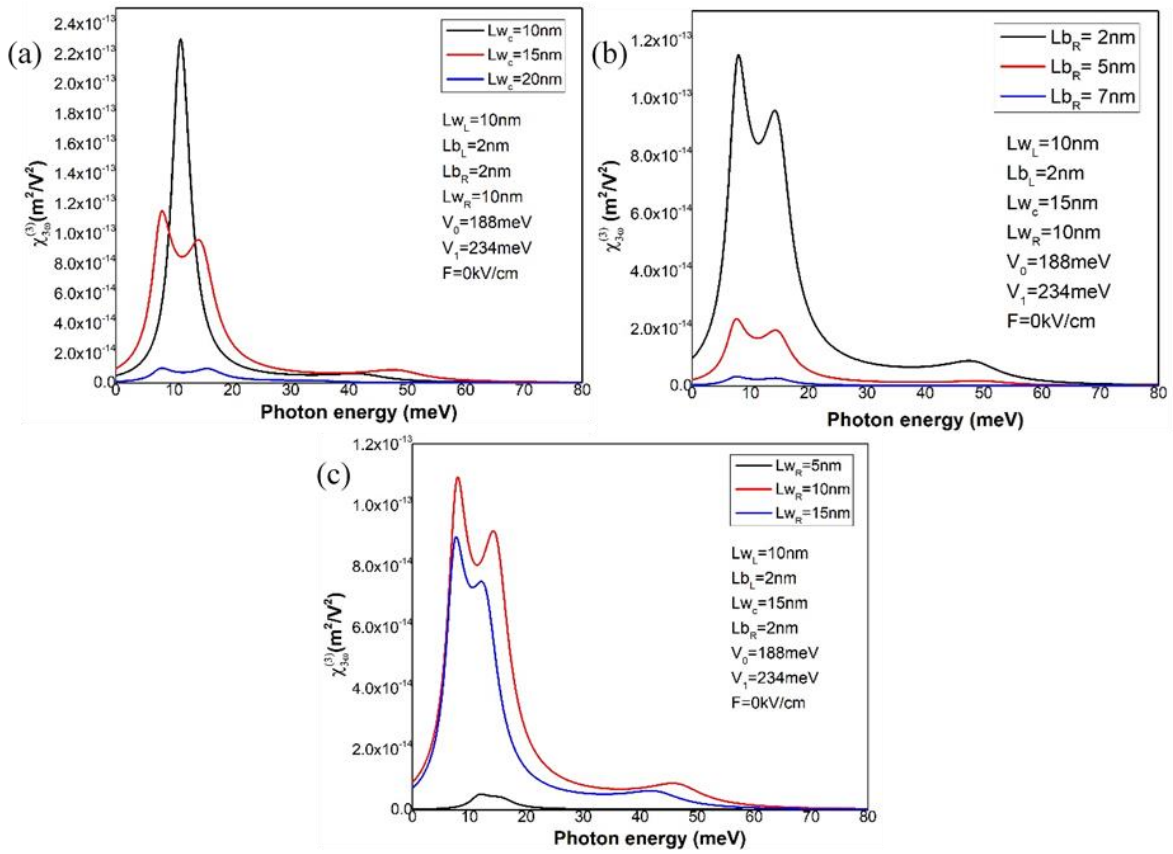

Figure 7. *Third harmonic generation coefficient as a function of incident light energy for different sets of structure parameters (a) Lw_c (b) Lb_R (c) Lw_R.*

The THG coefficient as a function of incident photon energy ($\hbar\omega$) is presented in Figure 7 for different structure parameters. The position of resonant peaks depends on the energy differences between the ground state and the first three excited states. The variation of the energy difference is seen in Figure 2. Figure 7(a) demonstrates the resonant THG coefficient for different center well width (Lw_c) values. Figure 7(b) exhibits the THG coefficient for different right well barrier (Lb_R) values. Figure 7 (c) is for THG coefficients for different right-well width (Lw_R) values. The variation of the structure parameters results in the change of energy difference between electron ground and first excited states. This produces displacements of THG coefficient resonant peak positions. The amplitude of the THG coefficient is, then, influenced by the product of the dipole moment matrix elements.

In Figure 8, the applied electric field (F) affects the THG coefficient's peak position. The main resonant peak position slightly shifts toward higher energies since the energy difference (E_{30}) increases with the increment of the applied F field. The amplitude of the resonant peak decreases as F increases due to the product of the dipole moment matrix elements. The main reason for these behaviors is the change in the energy difference and the overlap of states with the potential structure. The electrons' localization is compressed or expanded. Thus, the overlapping increases or decreases.

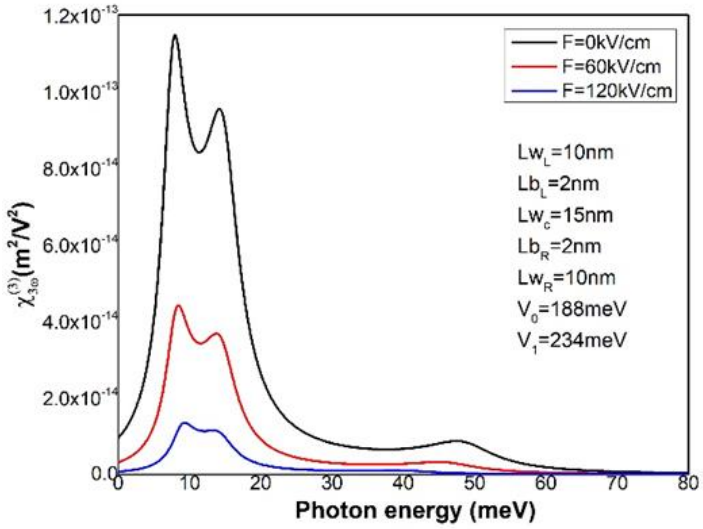

Figure 8. *The same as in Figure 7 but for different external electric field values.*

For Figures 5-8, double (for SHG) and triple (for THG) peaks are observed. For Fig. 5-6, the two-photon condition is not satisfied, and two peaks are observed. In the case of THG in Fig. 7-8, three-photon resonance is not satisfied, so triple peaks may be observed. The variation of the energy levels (ΔE) is seen in Fig. 2. In general, the physical origin of this behavior of nonlinear optical coefficients (NOR, SHG, and THG) is due to the quantum confinement effect. By changing the structure parameters and the applied external fields, the quantum confinement effects change. So the energy difference and the overlaps of states change. Electron localization is a crucial factor in studying the optical properties and understanding the behavior of the structure. This change allows the redshift or blueshift of the nonlinear optical properties of the structure.

3. CONCLUSION

In the present work, the nonlinear optical rectification coefficient (NOR), second harmonic generation (SHG), and third harmonic generation (THG) of a triple $In_xGa_{1-x}As/GaAs$ quantum well has been investigated. The energy levels and wave functions are obtained using a numerical method. The optical properties are obtained using the density matrix approach. The structure parameters and the applied external electric field modify the electron energy levels inside the confinement potential. The variations of the energy separation E_{10}, E_{20}, E_{30} and their dependence on the quantum size of different quantum wells and barriers as well as the electric field were discussed in detail. The resonant peak positions in the NOR, SHG, and THG move to a lower or higher energy region as the variation of the structure parameters and the external electric field. The magnitude of these coefficients decreases or increases as well. The structure parameters and the external electric field play a crucial role in controlling the optical properties of the used structure. The simulation results are useful in understanding the carrier dynamic of triple quantum well and provide detailed information for the design and fabrication of $In_xGa_{1-x}As/GaAs$-based optoelectronic devices operating in the infrared and far-infrared regions. In particular, the use of simulation results can help device designers optimize the structure and composition of the materials used in the triple quantum well, as well as optimize the device geometry and operating conditions. This can lead to more efficient and effective optoelectronic devices operating in the infrared and far-infrared regions, which can have important

applications in fields such as telecommunications, sensing, and imaging.

CONFLICT OF INTEREST

The authors declare that they have no conflict of interest.

DATA AVAILABILITY STATEMENT

This manuscript has associated data in a data repository. Data will be made available on request.

REFERENCES

1. Khordad, R., "Effects of magnetic field and geometrical size on the interband light absorption in a quantum pseudodot system", *Solid State Sciences*, 12 (2010) 1253-1256.
2. Şahin, M., "Third-order nonlinear optical properties of a one- and two-electron spherical quantum dot with and without a hydrogenic impurity", *Journal of Applied Physics*, 106 (2009) 063710.
3. Lu, L., Xie, W., Hassanabadi, H., "The effects of intense laser on nonlinear properties of shallow donor impurities in quantum dots with the Woods–Saxon potential", *Journal of Luminescence*, 131 (2011) 2538-2543.
4. Dakhlaoui, H., Nefzi, M., "Tuning the linear and nonlinear optical properties in double and triple δ− doped GaAs semiconductor: Impact of electric and magnetic fields", *Superlattices and Microstructures*, 136 (2019) 106292.
5. Karabulut, I., Paspalakis, E., "The role of permanent dipoles on the intensity-dependent nonlinear optical properties in asymmetric coupled quantum wells under a static electric field", *Physica E: Low-dimensional Systems and Nanostructures*, 81 (2016) 294-301.
6. Kria, M., El-Yadri, M., Aghoutane, N., Pérez, L. M., Laroze, D., Feddi, E., "Forecasting and analysis of nonlinear optical responses by tuning the thickness of a doped hollow cylindrical quantum dot", *Chinese Journal of Physics*, 66 (2020) 444-452.
7. Wang, G. H., Guo, Q., Guo, K. X., "Third-order nonlinear optical properties of parabolic and semiparabolic quantum wells", *Physica Status Solidi B*, 238 (2003) 75-80.
8. Feddi, E., Assaid, E., Dujardin, F., Stébé, B., Diouri, J., "Magnetic Field Influence on the Polarisability of Donors in Quantum Crystallites", *Physica Scripta*, 62 (2000) 88.
9. Rajaei, E., Borji, M. A., "Energy Levels of InGaAs/GaAs Quantum Dot Lasers with Different Sizes", *International Journal of Nanoscience and Nanotechnology*, 12 (2016) 45-53.
10. Wang, G. H., Guo, Q., Guo, K. X., "Refractive Index Changes Induced by the Incident Optical Intensity in Semiparabolic Quantum Wells", *Chinese Journal of Physics*, 41 (2003) 296-306.
11. Liang, S., Xie, W., Shen, H., "Optical properties in a two-dimensional quantum ring: Confinement potential and Aharonov–Bohm effect", *Optics Communications*, 284 (2011) 5818-5828.
12. Shao, S., Guo, K. X., Zhang, Z. H., Li, N., Peng, C., "Studies on the third-harmonic generations in cylindrical quantum dots with an applied electric field", *Superlattices and Microstructures*, 48 (2010) 541-549.
13. Kasapoglu, E., Duque, C. A., Sari, H., Sökmen, I., "Intense laser field effects on the linear and nonlinear intersubband optical properties of a semi-parabolic quantum well", *The European Physical Journal B*, 82 (2011) 13-17.
14. Pal, S., Ghosh, M., "Tailoring nonlinear optical rectification coefficient of impurity doped quantum dots by invoking Gaussian white noise", *Optical and Quantum Electronics*, 48 (2016) 372.
15. Arif, S. M., Bera, A., Ghosh, A., Ghosh, M., "Analyzing role of relaxation time on second harmonic generation and optical dielectric function of impurity doped quantum dots under the aegis of noise", *Physica B: Condensed Matter*, 588 (2020) 412166.
16. Ganguly, J., Ghosh, M., "Modulating optical second harmonic generation of impurity-doped quantum dots in presence of Gaussian white noise", *Physica Status Solidi B*, 253 (2016) 1093-1103.
17. Dujardin, F., Oukerroum, A., Feddi, E., Bailach, J. B., Pastor, J. M., Zazi, M., "Effect of a lateral electric field on an off-center single dopant confined in a thin quantum disk", *Journal of Applied Physics*, 111 (2012).
18. Khamkhami, J. E., Feddi, E., Assaid, E., Dujardin, F., Stébé, B., Diouri, J., "Binding energy of excitons in inhomogeneous quantum dots under uniform electric field", *Physica E: Low-dimensional Systems and Nanostructures*, 15 (2002) 99-106.
19. Yu, Y. B., Wang, H. J., "Third-harmonic generation in two-dimensional pseudo-dot system with an applied magnetic field", *Superlattices and Microstructures*, 50 (2011) 252-260.
20. Gravé, I., Segev, M., Yariv, A., "Observation of phase conjugation at 10.6 μm via intersubband third-order nonlinearities in a GaAs/AlGaAs multi-quantum-well structure", *Applied Physics Letters*, 60 (1992) 2717-2719.
21. Saha, S., Ghosh, M., "Tuning third harmonic generation of impurity doped quantum dots in the presence of Gaussian white noise", *Journal of Physics and Chemistry of Solids*, 90 (2016) 69-79.

22. Ganguly, J., Saha, S., Bera, A., Ghosh, M., "Modulating optical rectification, second and third harmonic generation of doped quantum dots: Interplay between hydrostatic pressure, temperature and noise", *Superlattices and Microstructures*, 98 (2016) 385-399.
23. Duque, C. A., Mora-Ramos, M. E., Barseghyan, M. G., "Electronic states in a Pöschl–Teller-like quantum well: Combined effects of electric field, hydrostatic pressure, and temperature", *Superlattices and Microstructures*, 50 (2011) 480-490.
24. Hakimyfard, A., Barseghyan, M. G., Kirakosyan, A. A., "Simultaneous effects of pressure and magnetic field on intersubband optical transitions in Pöschl–Teller quantum well", *Physica E: Low-dimensional Systems and Nanostructures*, 41 (2009) 1596-1599.
25. Barseghyan, M. G., Hakimyfard, A., Zuhair, M., Duque, C. A., Kirakosyan, A.A., "Binding energy of hydrogen-like donor impurity and photoionization cross-section in InAs Pöschl–Teller quantum ring under applied magnetic field", *Physica E: Low-dimensional Systems and Nanostructures*, 44 (2011) 419-424.
26. Radovanović, J., Milanović, V., Ikonić, Z., Indjin, D., "Intersubband absorption in Pöschl–Teller-like semiconductor quantum wells", *Physics Letters A*, 269 (2000) 179-185.
27. Yuh, P. F., Wang, K. L., "Optical transitions in a step quantum well", *Journal of Applied Physics*, 65 (1989) 4377-4381.
28. Hao, F., Pang, J. P., Sugiyama, M., Tada, K., Nakano, Y., "Field-induced optical effect in a five-step asymmetric coupled quantum well with modified potential", *IEEE Journal of Quantum Electronics*, 34 (1998) 1197-1208.
29. Yıldırım, H., Tomak, M., "Nonlinear optical properties of a Pöschl-Teller quantum well", *Physical Review B*, 72 (2005) 115340.
30. Restrepo, R. L., Ungan, F., Kasapoglu, E., Mora-Ramos, M. E., Morales, A. L., Duque, C. A., "The effects of intense laser field and applied electric and magnetic fields on optical properties of an asymmetric quantum well", *Physica B: Condensed Matter*, 457 (2015) 165-171.
31. Martínez-Orozco, J. C., Rodríguez-Magdaleno, K. A., Suárez-López, J. R., Duque, C. A., Restrepo, R. L., "Absorption coefficient and relative refractive index change for a double δ-doped GaAs MIGFET-like structure: Electric and magnetic field effects", *Superlattices and Microstructures*, 92 (2016) 166-173.
32. Kasapoglu, E., Sakiroglu, S., Sökmen, I., Restrepo, R. L., Mora-Ramos, M. E., Duque, C. A., "The effects of the electric and intense laser field on the binding energies of donor impurity states (1s and 2p±) and optical absorption between the related states in an asymmetric parabolic quantum well", *Optical Materials*, 60 (2016) 318-323.
33. Altun, D., Ozturk, O., Alaydin, B. O., Ozturk, E., "Linear and nonlinear optical properties of a superlattice with periodically increased well width under electric and magnetic fields", *Micro and Nanostructures*, 166 (2022) 207225.
34. Aydinoglu, H. S., Sayrac, M., Mora-Ramos, M. E., Ungan, F., "Nonlinear optical properties in AlxGa1-xAs/GaAs double-graded quantum wells: The effect of the structure parameter, static electric, and magnetic field", *Solid State Communications*, 342 (2022) 114647.
35. Sayrac, M., Turkoglu, A., Ungan, F. "Influence of hydrostatic pressure, temperature, and terahertz laser field on the electron-related optical responses in an asymmetric double quantum well", *The European Physical Journal B*, 94 (2021) 121.
36. Feddi, E., Zouitine, A., Oukerroum, A., Dujardin, F., Assaid, E., Zazoui, M., "Size dependence of the polarizability and Haynes rule for an exciton bound to an ionized donor in a single spherical quantum dot", *Journal of Applied Physics*, 117 (2015) 064309.
37. Gurnick, M., DeTemple, T., "Synthetic nonlinear semiconductors", *IEEE Journal of Quantum Electronics*, 19 (1983) 791-794.
38. Rosencher, E., Bois, P., "Model system for optical nonlinearities: Asymmetric quantum wells", *Physical Review B*, 44 (1991) 11315-11327.
39. Karabulut, I., Safak, H., Tomak, M., "Nonlinear optical rectification in asymmetrical semiparabolic quantum wells", *Solid State Communications*, 135 (2005) 735-738.
40. Baskoutas, S., Paspalakis, E., Terzis, A. F., "Electronic structure and nonlinear optical rectification in a quantum dot: effects of impurities and external electric field", *Journal of Physics: Condensed Matter*, 19 (2007) 395024.
41. Alaydin, B. O., "Effect of high bandgap AlAs quantum barrier on electronic and optical properties of In0.70Ga0.30As/Al0.60In0.40As superlattice under applied electric field for laser and detector applications", *International Journal of Modern Physics B*, 35 (2021) 2150027.
42. Sayrac, M., Turkoglu, A., Mora-Ramos, M. E., Ungan, F., "Intensity-dependent nonlinear optical properties in an asymmetric Gaussian potential quantum well-modulated by external fields", *Optical and Quantum Electronics*, 53 (2021) 485.

43. Kaynar, E., Alaydin, B. O., “Optical properties of AlxInyGa1−x−yAs/AlzGawIn1−z−wAs quantum wells under electric and magnetic fields for telecommunication applications”, *The European Physical Journal Plus*, 138 (2023) 121.
44. Dakhlaoui, H., Vinasco, J. A., Duque, C. A., “External fields controlling the nonlinear optical properties of quantum cascade laser based on staircase-like quantum wells”, *Superlattices and Microstructures*, 155 (2021) 106885.
45. Turkoglu, A., Dakhlaoui, H., Mora-Ramos, M. E., Ungan, F., “Optical properties of a quantum well with Razavy confinement potential: Role of applied external fields”, *Physica E: Low-dimensional Systems and Nanostructures*, 134 (2021) 114919.
46. Sakiroglu, S., Yesilgul, U., Ungan, F., Duque, C. A., Kasapoglu, E., Sari, H., Sokmen, I., “Electronic band structure of GaAs/AlxGa1−xAs superlattice in an intense laser field”, *Journal of Luminescence*, 132 (2012) 1584-1588.
47. Ungan, F., Yesilgul, U., Şakiroğlu, S., Kasapoglu, E., Sari, H., Sökmen, I., “Effects of an intense, high-frequency laser field on the intersubband transitions and impurity binding energy in semiconductor quantum wells”, *Physics Letters A*, 374 (2010) 2980-2984.
48. Eseanu, N., “Simultaneous effects of laser field and hydrostatic pressure on the intersubband transitions in square and parabolic quantum wells”, *Physics Letters A*, 374 (2010) 1278-1285.
49. Mora-Ramos, M. E., Duque, C. A., Kasapoglu, E., Sari, H., Sökmen, I., “Electron-related nonlinearities in GaAs–Ga1−xAlxAs double quantum wells under the effects of intense laser field and applied electric field”, *Journal of Luminescence*, 135 (2013) 301-311.
50. Ünlü, S., Karabulut, İ., Şafak, H., “Linear and nonlinear intersubband optical absorption coefficients and refractive index changes in a quantum box with finite confining potential”, *Physica E: Low-dimensional Systems and Nanostructures*, 33 (2006) 319-324.
51. Doyeol, A., Shun-lien, C., “Calculation of linear and nonlinear intersubband optical absorptions in a quantum well model with an applied electric field”, *IEEE Journal of Quantum Electronics*, 23 (1987) 2196-2204.
52. Martínez-Orozco, J. C., Mora-Ramos, M. E., Duque, C. A., “Nonlinear optical rectification and second and third harmonic generation in GaAs δ-FET systems under hydrostatic pressure”, *Journal of Luminescence*, 132 (2012) 449-456.
53. Mora-Ramos, M. E., Duque, C. A., Kasapoglu, E., Sari, H., Sökmen, I., “Linear and nonlinear optical properties in a semiconductor quantum well under intense laser radiation: Effects of applied electromagnetic fields”, *Journal of Luminescence*, 132 (2012) 901-913.
54. Sayrac, M., Kaynar, E., Ungan, F., “The effect of structure parameters and static electric field on the nonlinear optical properties of triple InGaAs/GaAs quantum well”, *Journal of Molecular Structure*, (2022) 134252.
55. Sayrac, M., “Effects of applied external fields on the nonlinear optical rectification, second, and third-harmonic generation in an asymmetrical semi exponential quantum well”, *Optical and Quantum Electronics*, 54 (2021) 52.
56. Ozturk, O., Ozturk, E., Elagoz, S., “Linear and nonlinear optical absorption coefficient and electronic features of triple GaAlAs/GaAs and GaInAs/GaAs quantum wells depending on barrier widths”, *Optik*, 180 (2019) 394-405.